NANO LETTERS

Letter

pubs.acs.org/NanoLett

Revealing Energy Level Structure of Individual Quantum Dots by Tunneling Rate Measured by Single-Electron Sensitive Electrostatic Force Spectroscopy

Antoine Roy-Gobeil, Yoichi Miyahara,* and Peter Grutter

Department of Physics, McGill University, 3600 rue University, Montreal, Quebec H3A2T8, Canada

Supporting Information

ABSTRACT: We present theoretical and experimental studies of the effect of the density of states of a quantum dot (QD) on the rate of single-electron tunneling that can be directly measured by electrostatic force microscopy (e-EFM) experiments. In e-EFM, the motion of a biased atomic force microscope cantilever tip modulates the charge state of a QD in the Coulomb blockade regime. The charge dynamics of the dot, which is detected through its back-action on the capacitively coupled cantilever, depends on the tunneling rate of the QD to a back-electrode. The density of states of the QD can therefore be measured through its effect on the energy dependence of tunneling rate. We present experimental data on individual 5 nm colloidal gold nanoparticles that exhibit a near continuous density of state at 77 K. In contrast, our analysis of already published data on self-assembled InAs QDs at 4 K clearly reveals discrete degenerate energy levels.

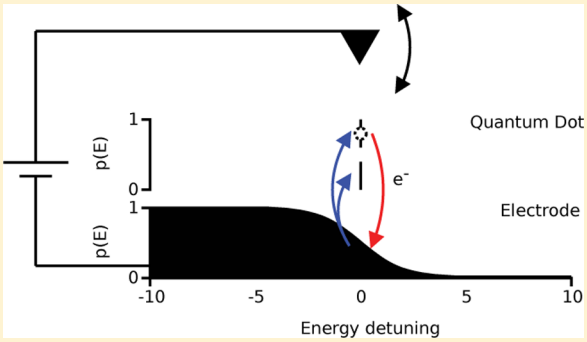

KEYWORDS: *Quantum dot, Coulomb blockade, singe-electron tunneling, atomic force microscopy, tunneling spectroscopy, nanoparticle*

Quantum dots (QDs) have attracted a lot of interest in the past decades due to their novel electronic, optical, and chemical properties. Of particular interest is their ability to control the number of confined electrons precisely when isolated by a tunnel barrier, which may lead to their incorporation in nanoelectronic devices.[1]

Tremendous progress has been made to measure the electronic properties of various QDs such as electronic level structure and charging energy via various single-electron transport measurements including dc current measurement,[2] charge sensing,[3] and capacitance/admittance spectroscopy.[4,5] In these measurements, a series of peaks are observed in the measured signal versus gate voltage curves (Coulomb peaks). Although the separation of the peaks are indicative of the energy level structure, revealing the detail of electronic level structure such as identifying degenerate levels requires elaborate experiments that involve measurements with varying applied magnetic field[6,7] in order to separate the single-electron charging energy from the observed peak separations. Energy level spectroscopy has been possible only when the energy separation, ΔE_{level}, is much larger than thermal energy, k_BT.

Scanning tunneling spectroscopy (STS) has also been successfully applied for energy level spectroscopy of colloidal QDs.[8−10] As such STS experiments need to be performed in double-barrier tunnel junction systems to measure a dc tunneling current, its applicability is thus limited to systems where a reliable tip-QD tunnel junction can be realized and the QD-substrate tunnel junction is transparent enough for a detectable tunneling current (typically >1 pA). The former condition often requires a clean sample surface to be measured in ultrahigh vacuum condition, limiting the kind of QDs which can be studied.

Electrostatic force microscopy with single-electron sensitivity (e-EFM) has been developed as an alternative way to probe single-electron transport in broader ranges of QDs such as epitaxially grown self-assembled and colloidal ones to which patterned electrodes are much more difficult to attach.[11−13] e-EFM technique alleviates this problem by using an oscillating atomic force microscopy (AFM) probe as a movable charge sensor as well as gate electrode. The technique yields peaks in the cantilever's resonance frequency shift and damping versus bias voltage curves (referred to as e-EFM spectra, hereafter) caused by single-electron tunneling, which carry the same information as Coulomb peaks measured in the above-mentioned transport measurements. Because it retains the imaging capabilities of AFM, it enables a systematic exploration of structure−property relationships, which is of central interest in nanotechnology.

In contrast with other single-electron charge detection experiments done by AFM[14,15] e-EFM technique provides not only the charge state of the sample but also the dynamics of tunneling single electrons, which enables quantitative spectroscopic measurement of energy level structure. For instance,

Received: November 20, 2014
Revised: March 5, 2015
Published: March 11, 2015

DOI: 10.1021/nl504468a
Nano Lett. 2015, 15, 2324−2328

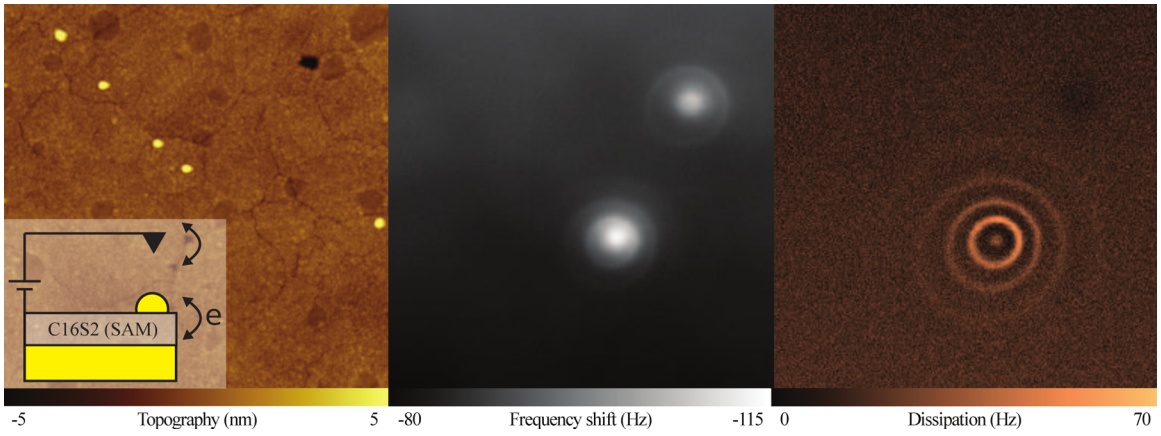

Figure 1. (Left) The 1 μm^2 tapping mode topography image of 5 nm Au colloidal nanoparticles on a self-assembled monolayer of 1,16-hexadecanedithiol (C16S2). (Inset) Schematic of the oscillating cantilever with tip pushing electrons on and off the QD when the bias voltage is enough to lift the Coulomb blockade. (Center and right) Simultaneously recorded frequency shift and dissipation images (200 nm by 200 nm) acquired at constant-height over two 5 nm Au nanoparticles with an applied tip bias of 7.7 V at 77 K. Peak-to-peak oscillation amplitude was 1 nm.

Cockins et al.[12] and Bennett et al.[16] demonstrated that degenerate energy levels can be revealed by measuring the temperature dependence or oscillation amplitude dependence of the e-EFM spectra. Excited energy levels have also been measured.[17]

In this Letter, we show an alternative route to obtain such spectroscopic information by measuring the bias voltage-dependent tunneling rate (tunneling rate spectrum), which can be measured easily by e-EFM technique. Fitting the experimental tunneling rate spectrum with the theoretical one using standard single-electron tunneling transport theory[18] has the potential to reveal the electronic energy level structure (density of states) of the QD even in the condition, $k_BT \gg \Delta E_{level}$ where the effect of ΔE_{level} on the peak separations are not discernible.

Measurements performed on 5 nm colloidal gold nanoparticles (GNP) at 77 K reveals a near continuous density of states. We then apply our analysis to already published data on self-assembled InAs QD measured at 4 K and show that degeneracies and shell-filling can be identified straightforwardly from a single tunneling-rate spectrum obtained from a single pair of frequency shift and dissipation peaks without performing variable temperature[12] or magnetic field experiments.

In e-EFM, electron tunneling into and out of QDs happens through a single tunnel barrier while an AFM cantilever tip capacitively coupled to the QD is used both as a gate and charge sensor.[19] Tunneling between the back-electrode and QD is suppressed (Coulomb blockade) by the electrostatic energy cost (charging energy), E_C, of adding or removing an electron to the QD except near charge degeneracy points at which two successive charge states share the same energy.

A dc-bias voltage, V_B, is applied to the tip with respect to the grounded back-electrode (see inset of Figure 1A) to overcome E_C. The potential drop, αV_B ($\alpha < 1$), across the tunnel barrier between the QD and the back-electrode determines the tunneling process and is only a fraction of V_B with lever arm, $\alpha(x,y,z) = C_{tip}/C_\Sigma$, being a function of the tip-QD capacitance, $C_{tip}(x,y,z)$, and total dot capacitance $C_\Sigma = C_{tip} + C_{2DEG}$ where the coordinate, (x,y) and z, denotes the lateral and vertical position of the tip with respect to the QD, respectively.

For a small vertical cantilever tip motion compared to the average tip−QD distance, $C_{tip}(x,y,z)$ varies linearly with z and we can write the charging Hamiltonian of the dot as[20]

$$\mathcal{H} = E_C[(n - \mathcal{N})^2 - \left(\frac{1 - C_{2DEG}}{C_{tip}}\right)\mathcal{N}^2] \simeq \mathcal{H}_{C,0} + Anz$$

where $\mathcal{H}_{C,0}$ is an oscillator-independent part of the Hamiltonian, n is the number of electrons on the QD, $E_C = e^2/2C_\Sigma$ is the charging energy, and $A = -(2E_CV_B/e)(1-\alpha)\partial C_{tip}/\partial z$ is the dot-cantilever coupling strength.[12] e-EFM experiments are performed in frequency modulation mode in which the cantilever oscillates at constant amplitude, a, and at its resonance frequency. In this mode, the oscillation of the cantilever tip modulates $\alpha(x,y,z)$ that leads to an effective oscillating gate voltage applied to the QD. At charge degeneracy points, this results in a modulation of the charge of the QD in response to the cantilever motion. The changes in the resonance frequency and dissipation, caused by the resultant ac electrostatic force, can be measured with high sensitivity using frequency modulation techniques.[21]

We model the time evolution of the charge state of the QD and the resulting back-action force in a regime where 0 or 1 extra electrons can reside on the QD with other charge states prohibited by Coulomb blockade. Within the orthodox model,[22] its state can be described by the probability $P(t)$ of having an extra electron at time t. The evolution of this probability in time can be described by the following mean-field master equation[16]

$$\partial_t\langle P\rangle = -\Gamma_-(\langle z\rangle)\langle P\rangle + \Gamma_+(\langle z\rangle)(1 - \langle P\rangle) \quad (1)$$

where $\Gamma_+(\Gamma_-)$ are z-dependent tunneling rates to add (remove) an electron to the QD. Because of the finite tunneling rate of electrons, $\langle P(t)\rangle$ is out of phase with respect to the cantilever oscillation, $\langle z(t)\rangle = a \cos \omega_0 t$, which results in a back-action force that causes a change in both its resonance frequency, $\Delta\omega/2\pi$, and its dissipation, $\Delta\gamma$, with magnitudes

$$\Delta\omega = -\frac{\omega_0 A}{2\pi k_0 a}\int_0^{2\pi/\omega_0} dt\, \cos(\omega_0 t)\langle P(t)\rangle \quad (2)$$

$$\Delta\gamma = \frac{\omega_0^2 A}{\pi k_0 a}\int_0^{2\pi/\omega_0} dt\, \sin(\omega_0 t)\langle P(t)\rangle \quad (3)$$

DOI: 10.1021/nl504468a
Nano Lett. 2015, 15, 2324−2328

Table 1. Functional Form of Tunneling Rate Equations in Limiting Cases Obtained from Equations 7 and 8

case	Γ_+	Γ_-	Γ_Σ
single nondegenerate level	$\Gamma f(\Delta E)$	$\Gamma(1 - f(\Delta E))$	Γ
single degenerate level	$(\nu - n_{\mathrm{shell}})\Gamma f(\Delta E)$	$(n_{\mathrm{shell}} + 1)\Gamma(1 - f(\Delta E))$	$(\nu - n_{\mathrm{shell}})\Gamma f(\Delta E) + (n_{\mathrm{shell}} + 1)\Gamma(1 - f(\Delta E))$
continuous density of states	$\Gamma\rho(1/2)[(-\beta\Delta)/(1-e^{\beta\Delta E})]$	$\Gamma\rho(1/2)[(\beta\Delta E)/(1-e^{-\beta\Delta E})]$	$\Gamma\rho(1/2)\beta\Delta E\coth[(1/2)\beta\Delta E]$

where k_0 and ω_0 are the spring constant and resonance frequency of the cantilever, respectively and the values with $\langle\rangle$ denote their expectation value.

In the regime of weak coupling ($aA \ll k_BT$), tunneling rates vary linearly with z, and the above expressions reduce to

$$\Delta\omega = -\frac{\omega_0 A^2}{2k_0}\frac{(\Gamma'_+\Gamma_\Sigma - \Gamma_+\Gamma'_\Sigma)}{(\Gamma_\Sigma^2 + \omega^2)} \tag{4}$$

$$\Delta\gamma = \frac{\omega_0^2 A^2}{k_0\Gamma_\Sigma}\frac{(\Gamma_+'\Gamma_\Sigma - \Gamma_+\Gamma'_\Sigma)}{(\Gamma_\Sigma^2 + \omega^2)} \tag{5}$$

where $\Gamma_\Sigma = \Gamma_+ + \Gamma_-$ is the total tunneling rate and $'$ denotes derivative with respect to energy. The total tunneling rate between the QD and the back-electrode, Γ_Σ, can be directly measured as a function of the electrochemical potential detuning by noting that

$$\Gamma_\Sigma = -2\omega_0\frac{\Delta\omega}{\Delta\gamma} \tag{6}$$

It is by virtue of this relation that the measurement of the energy-dependent tunneling rate is straightforward with e-EFM technique, whereas the conventional transport measurement does not allow this measurement easily. To extract the electronic level structure of the QD from the experimentally obtained energy dependence of Γ_Σ, we rely on standard single-electron tunneling transport theory.[18] Using Fermi's golden rule, the electron tunneling rate between the QD and back-electrode are given by the following summations over all energy levels, k, of the QD with respective coupling strength to the electrode, Γ_k, and energy E_k

$$\Gamma_+ = \sum_k \Gamma_k[1 - F_{\mathrm{eq}}(E_k|n-1)]f(E_k + \Delta E) \tag{7}$$

$$\Gamma_- = \sum_k \Gamma_k F_{\mathrm{eq}}(E_k|n)[1 - f(E_k + \Delta E)] \tag{8}$$

where ΔE is the electrochemical potential difference between the QD and electrode is determined by αV_B. f is the Fermi distribution function and $F_{\mathrm{eq}}(E_k|n)$ is the conditional probability of having level k occupied when n electrons are contained in the QD in equilibrium. Those expressions reduce to analytical solutions under certain conditions which we summarize in Table 1.

In the limit of high temperature ($k_BT \gg \Delta E_{\mathrm{level}}$, classical regime), the discrete energy spectrum of the QD may be treated as a continuum of energy levels with density of states, ρ, and one may approximate $F_{\mathrm{eq}}(E_k|n)$ by the Fermi–Dirac distribution.[18] By neglecting the energy dependence of the density of states, ρ, and of the tunnel coupling strength, $\Gamma_k \equiv \Gamma$, the tunneling rates reduce to $\Gamma_\Sigma = \Gamma\rho(1/2)\beta\Delta E\coth(1/2\beta\Delta E)$ where $\beta = 1/k_BT$. The calculation also greatly simplifies in the limit of low temperature, ($k_BT \ll \Delta E_{\mathrm{level}}$, quantum regime), where electrons fill the QD up to the Fermi level and $F_{\mathrm{eq}}(E_n|n) = 1$. In this case, the total tunneling rate $\Gamma_\Sigma = \Gamma_+ + \Gamma_-$ is constant for a single nondegenerate energy level. Table 1 also contains formulas for the tunneling rates involved with ν-fold degenerate levels with shell-filling n_{shell} assuming constant Γ_k.[12] The expected total tunneling rate for cases relevant to our measurements are plotted in Figure 2 (see animated figures in the Supporting Information).

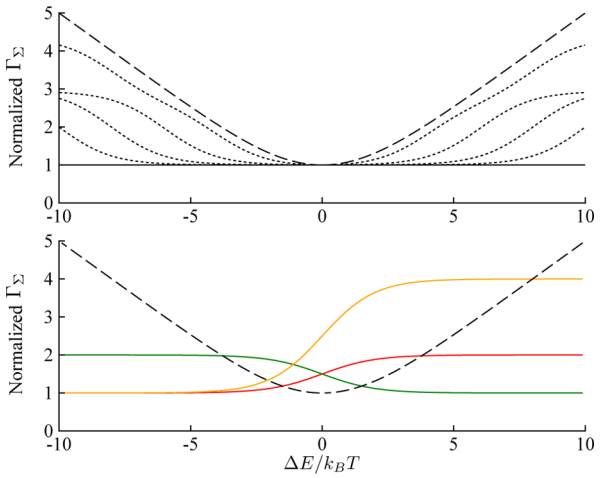

Figure 2. Theoretical total tunneling rate as a function of electrochemical potential detuning ΔE. (Top) QD with an infinite number of equally spaced nondegenerate energy levels. The solid line is for a single nondegenerate level (flat) and the long-dashed line is for a continuous density of states with $\rho = 1$. Short-dashed lines are numerically evaluated for energy level spacing of 4, 6, 8, and 10 k_BT assuming $F_{\mathrm{eq}}(E_k|n) = f$ for simplicity. (Bottom) QD with a single degenerate level. A 2-fold degenerate level yields the red and green curves with respective shell-filling, n_{shell}, equals to 0 and 1. The orange curve is for a 4-fold degenerate level with $n_{\mathrm{shell}} = 0$.

We stress that although the expressions for the tunneling rate greatly simplify for those cases, the utility of the technique is not limited to them. On the contrary, by tuning the parameters of eqs 7 and 8 and numerically computing the associated tunneling rates, more accurate and detailed energy level structure can be obtained from the measurements. For example, measuring the transition from high to low tempearture limit has the potential of revealing the electron distribution, $F_{\mathrm{eq}}(E_k|n)$, at intermediate temperatures.[18]

Experimentally, in order to achieve sufficient signal-to-noise ratio, it is ideal to operate in a regime where the cantilever's response is evenly split between $\Delta\omega$ and $\Delta\gamma$. This condition is met when the effective tunneling rate matches the resonance frequency of the cantilever.[11,13] Because mechanical oscillators typically have a fixed ω_0, one usually needs to adjust the tunneling rate of the barrier to achieve this condition.

For the study of GNPs, alkanethiol molecules are a perfect candidate for the design of such barrier because of an exponential dependence of tunneling rate on the molecular length[23] and their high affinity for gold on which they are known to grow self-assembled monolayers (SAM). In this experiment, we show that a SAM of 1,16-hexadecanedithiol (C16S2) separating 5 nm GNPs from a Au back-electrode

DOI: 10.1021/nl504468a
Nano Lett. 2015, 15, 2324−2328

provides a tunneling rate that roughly matches the resonance frequency of our cantilever, $\omega_0/2\pi$ = 160 kHz. The sample was prepared by immersing a flat gold substrate in a solution of C16S2 at 1 mM for a few days. Finally, the substrate was immersed in a solution of 5 nm GNPs for them to chemisorb on the SAM (More detail is available in Supporting Information).

e-EFM experiment were performed with a home-built low temperature AFM.[24] The spring constant of the cantilever, k_0, is about 40 N/m and its quality factor (Q) varies between 15 000 and 50 000 depending on the temperature. The cantilever is self-excited at its resonant frequency by feedbacking its deflection signal into a piezoelectric excitation system via an oscillation control electronics. The oscillation amplitude is kept constant by controlling the amplitude of the cantilever excitation signal, A_{exc}, with a proportional integral controller. To compare acquired spectra to theory, the parabolic background due to the capacitive force between the tip and the back-electrode is subtracted from the experimental frequency shift versus bias voltage curve. For the dissipation measurements, the measured excitation amplitude is first compensated for the crosstalk due to the effect of the piezoacoustic transfer function by using the curves taken off the QDs[25] and then is converted to units of hertz via $(\omega_0/Q)[(A_{exc}/A_{exc0}) - 1]$ where A_{exc0} is the excitation amplitude with no tip−sample interaction (see more detail of the conversion in Supporting Information).

Scanning the tip over the GNPs/C16S2/Au sample at constant height and with a fixed bias voltage shows rings of constant αV_B in frequency shift images (Figure 1B) and dissipation (Figure 1C) that are due to single-electron tunneling through the C16S2 SAM layer. The circular ring shape originates from the fact that the lever arm, $\alpha(x, y, z)$, which determines chemical potential detuning, ΔE, is just a function of the distance between the QD and tip, $r = (x^2 + y^2 + z^2)^{1/2}$, such as $\alpha(x,y,z) = \alpha(r)$.[12] A pair of frequency shift and dissipation images such as shown in Figure 1B,C can provide the tunneling rate of each individual GNP. Out of nine GNPs that we measured, eight GNPs exhibit the rings both in $\Delta\omega$ and $\Delta\gamma$, which show the tunneling rate ranging from 110 to 830 kHz. (See Supporting Information for more detail.) The top GNP imaged in Figure 1B,C shows a rare but instructive instance in which dissipation rings are too faint to be detected, which is indicative of a tunneling rate >10 MHz.[26] This may be the result of the GNP sitting on a thinner and more transparent barrier which could indicate the presence of defects in the SAM. This demonstrates the ability of e-EFM technique to measure the tunneling rate of each individual QD just by taking a pair of $\Delta\omega$ and $\Delta\gamma$ images and using the relation shown in eq 6.

Spectrum acquired at 77 K on 5 nm GNPs shows single-electron tunneling events in both dissipation and frequency shift (see Figure 3). By fitting peaks with eqs 4 and 5, we obtain the lever-arm, α, of 0.064 and we measure a charging energy of 35 meV from the peak separation. The extracted total tunneling rate (Figure 3 bottom) shows a clear signature of tunneling involving multiple levels in the QD as shown in Figure 2 and is in a good agreement with the analytical expression assuming a continuous density of states.

In order to demonstrate the generality and simplicity of this spectroscopy technique, we present similar measurements performed on epitaxially grown self-assembled InAs QDs on InP at 4 K (see ref 12 for experimental details). In this case, the

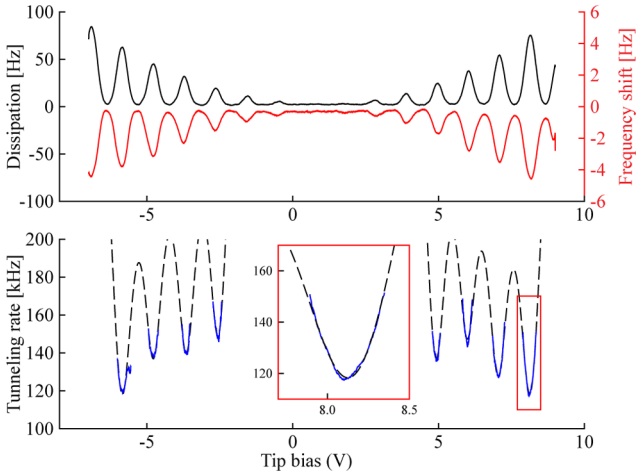

Figure 3. (Top) Experimental dissipation and frequency shift spectrum for 5 nm Au NP measured at 77 K. (Bottom) Extracted tunneling rate data (blue) superimposed with a fit to the analytical expression for a continuous density of states (dashed line).

total tunneling rate (Figure 4 bottom) shows a qualitatively different signature than in the classical regime. Looking at

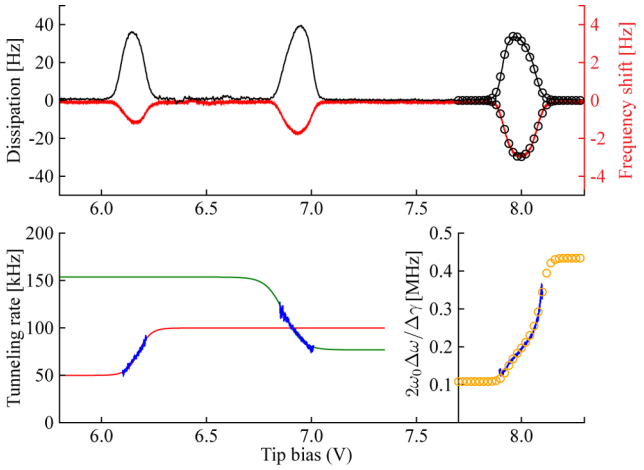

Figure 4. (Top) Experimental dissipation and frequency shift spectrum for InAs QD measured at 4 K. (Bottom) Corresponding tunneling rate data (blue) obtained from the data above superimposed with fits to tunneling rate expressions for 2-fold degenerate levels (color scheme from Figure 2 is reused). Circles are a best fit solution assuming tunneling into an empty 4-fold degenerate level and accounting for the effect of strong coupling.

Figure 2 bottom, we can easily tell it is indicative of electron tunneling into a single degenerate level of the QD. By fitting the data with the corresponding expression from Table 1, we find that the degeneracy, ν, has to be equal to 2 in order to properly fit the slope of Γ_Σ while the shell-filling, n_{shell}, is readily identified by the sign of the slope. This is in agreement with the results of a much more complicated measurement of a temperature-dependent level repulsion of peaks specific to this system.[12] At higher voltage, the weak coupling approximation start to break down and the ratio $2\omega_0\Delta\omega/\Delta\gamma$ is no longer equal to the tunneling rate Γ_Σ. Nevertheless, by looking at the slope of this ratio for the third peak, we can identify that tunneling occurs into an empty 4-fold degenerate level but to properly fit the data, we had to numerically solve eqs 1−3 to

DOI: 10.1021/nl504468a
Nano Lett. 2015, 15, 2324−2328

account for the effect of strong coupling.[16] The method described here enables to extract such valuable information just by analyzing a single pair of peaks.

In conclusion, we have shown that by performing tunneling rate spectroscopy, AFM can be used to measure the density of states or the electronic structure of individual QDs. The system is simpler than double barrier scanning tunneling spectroscopy as only a single tunnel junction is involved. Moreover, because tunneling only occurs between the QD and back-electrode, this technique does not require a clean surface. Samples can be exposed to air, which greatly relaxes the constraints associated with sample preparation and ultimately collaboration with other laboratories. Finally, we note that the results presented here can be applied to other capacitance/admittance spectroscopy techniques which are recently emerging[4−6,27] and the presented theoretical analysis is applicable to the other tunneling rate measurements by single-electron counting technique.[28]

■ ASSOCIATED CONTENT

Supporting Information

Detail of sample preparation, tunneling barrier engineering, conversion of dissipation in different units, animated figures of Figure 2. (i) Continuous density of states. (ii) Single nondegerante level. (iii) Single 2-fold degenerate level with zero electron occupancy. (iv) Single 2-fold degenerate level with one electron occupancy. This material is available free of charge via the Internet at http://pubs.acs.org.

■ AUTHOR INFORMATION

Corresponding Author

*E-mail: yoichi.miyahara@mcgill.ca. Phone: +1-514-398-6536. Fax:+1-514-398-8434.

Notes

The authors declare no competing financial interest.

■ ACKNOWLEDGMENTS

Funding was provided by the Natural Sciences and Engineering Research Council of Canada, le Fonds Québécois de le Recherche sur la Nature et les Technologies, and the Canadian Institute for Advanced Research.

■ REFERENCES

(1) Ray, V.; Subramanian, R.; Bhadrachalam, P.; Ma, L.-C.; Kim, C.-U.; Koh, S. J. *Nat. Nanotechnol.* **2008**, *3*, 603−8.
(2) Kouwenhoven, L.; Johnson, A.; van der Vaart, N.; Harmans, C.; Foxon, C. *Phys. Rev. Lett.* **1991**, *67*, 1626−1629.
(3) Field, M.; Smith, C. G.; Pepper, M.; Ritchie, D. A.; Frost, J. E. F.; Jones, G. A. C.; Hasko, D. G. *Phys. Rev. Lett.* **1993**, *70*, 1311−1314.
(4) Ashoori, R. C.; Stormer, H. L.; Weiner, J. S.; Pfeiffer, L. N.; Pearton, S. J.; Baldwin, K. W.; West, K. W. *Phys. Rev. Lett.* **1992**, *68*, 3088−3091.
(5) Colless, J. I.; Mahoney, A. C.; Hornibrook, J. M.; Doherty, A. C.; Lu, H.; Gossard, A. C.; Reilly, D. J. *Phys. Rev. Lett.* **2013**, *110*, 046805.
(6) Ashoori, R. C.; Stormer, H. L.; Weiner, J. S.; Pfeiffer, L. N.; Baldwin, K. W.; West, K. W. *Phys. Rev. Lett.* **1993**, *71*, 613−616.
(7) Tarucha, S.; Austing, D. G.; Honda, T.; van der Hage, R. J.; Kouwenhoven, L. P. *Phys. Rev. Lett.* **1996**, *77*, 3613−3616.
(8) Banin, U.; Cao, Y.; Katz, D.; Millo, O. *Nature* **1999**, *400*, 542−544.
(9) Banin, U.; Millo, O. *Annu. Rev. Phys. Chem.* **2003**, *54*, 465−92.
(10) Vanmaekelbergh, D.; Casavola, M. *J. Phys. Chem. Lett.* **2011**, *2*, 2024−2031.
(11) Zhu, J.; Brink, M.; McEuen, P. L. *Nano Lett.* **2008**, *8*, 2399−404.
(12) Cockins, L.; Miyahara, Y.; Bennett, S. D.; Clerk, A. A.; Studenikin, S.; Poole, P.; Sachrajda, A.; Grutter, P. *Proc. Natl. Acad. Sci. U.S.A.* **2010**, *107*, 9496−501.
(13) Tekiel, A.; Miyahara, Y.; Topple, J. M.; Grutter, P. *ACS Nano* **2013**, *7*, 4683−90.
(14) Gross, L.; Mohn, F.; Liljeroth, P.; Repp, J.; Giessibl, F. J.; Meyer, G. *Science* **2009**, *324*, 1428−1431.
(15) Mohn, F.; Gross, L.; Moll, N.; Meyer, G. *Nat. Nanotechnol.* **2012**, *08*, 1−5.
(16) Bennett, S. D.; Cockins, L.; Miyahara, Y.; Grütter, P.; Clerk, A. A. *Phys. Rev. Lett.* **2010**, *104*, 017203.
(17) Cockins, L.; Miyahara, Y.; Bennett, S. D.; Clerk, A. A.; Grutter, P. *Nano Lett.* **2012**, *12*, 709−13.
(18) Beenakker, C. W. J. *Phys. Rev. B* **1991**, *44*, 1646−1656.
(19) Tunneling between the tip and QD is negligible because of their large separation (>10 nm).
(20) Stomp, R.; Miyahara, Y.; Schaer, S.; Sun, Q.; Guo, H.; Grutter, P.; Studenikin, S.; Poole, P.; Sachrajda, A. *Phys. Rev. Lett.* **2005**, *94*, 056802.
(21) Albrecht, T. R.; Grütter, P.; Horne, D.; Rugar, D. *J. Appl. Phys.* **1991**, *69*, 668.
(22) Ferry, D.; Goodnick, S. *Transport in nanostructures*; Cambridge University Press: New York, 2009.
(23) Wang, W.; Lee, T.; Reed, M. A. *Phys. Rev. B* **2003**, *68*, 35416.
(24) Roseman, M.; Grüter, P. *Rev. Sci. Instrum.* **2000**, *71*, 3782.
(25) Labuda, A.; Miyahara, Y.; Cockins, L.; Grütter, P. *Phys. Rev. B* **2011**, *84*, 125433.
(26) Estimated from the dissipation noise.
(27) Frey, T.; Leek, P. J.; Beck, M.; Faist, J.; Wallraff, A.; Ensslin, K.; Ihn, T.; Büttiker, M. *Phys. Rev. B* **2012**, *86*, 115303.
(28) Müller, T.; Güttinger, J.; Bischoff, D.; Hellmüller, S.; Ensslin, K.; Ihn, T. *Appl. Phys. Lett.* **2012**, *101*, 012104.

DOI: 10.1021/nl504468a
Nano Lett. 2015, 15, 2324−2328